ARCHIVE OF MECHANICAL ENGINEERING

DOI: 10.24425/ame.2026.1884 Early Access; pp. 1–18

Mehdi JAFARI VARDANJANI [1], Alireza ARAEE [2]

Optimization of weld strength in indirect resistance welding of AISI 316L wires: A study on the synergistic effects of pulsed current and preheat temperature

Received 3 February 2026, **Revised** 5 May 2026, **Accepted** 26 May 2026, **Published online** 6 July 2026

Keywords: pulsed current frequency, preheating temperature, shear-tensile strength, heat-affected zone

This study investigates the enhancement of weld strength in indirect resistance welding of AISI 316L stainless steel wedge wires by systematically evaluating the effects of pulsed current frequency and preheating temperature. A comprehensive Design of Experiments (DOE) approach was employed, incorporating varying pulsation frequencies (0–10 Hz) and preheat temperatures (50–200°C), while maintaining constant welding current (7 kA) and time (25 cycles). Experimental and numerical analyses were conducted to assess shear-tensile strength and heat-affected zone (HAZ) depth. Results demonstrate that both pulsed current and elevated preheating contribute significantly to improved mechanical performance. Pulsation promoted localized energy concentration, reducing HAZ extent and enhancing joint strength, while preheating mitigated thermal gradients and residual stresses, further increasing load-bearing capacity. The combined application of optimized pulsation and preheating parameters proved effective in overcoming loose connections and achieving superior weld integrity, offering a reliable strategy for quality improvement in the resistance welding of fine metallic components.

1. Introduction

Resistance welding is a prevalent method for joining metallic components, valued for its speed and efficiency. In standard configurations, a point-to-point contact is often employed for prismatic wire-to-wire joints. However, specific applications, such as the assembly of wedge-shaped wires, necessitate unconventional

✉ Mehdi JAFARI VARDANJANI, e-mail: m-jafari@tvu.ac.ir

[1]Department of Mechanical Engineering, Technical and Vocational University (TVU), Tehran, Iran

[2]Schools of Mechanical Engineering, University of Tehran, North Kargar, Tehran, Iran

geometries like a reverse welding setup. In this configuration, the contact becomes point-to-back, where the sharp edge (point) of one wire is welded to the flat surface (back) of another. This asymmetric contact creates inherent challenges, including non-uniform current density, concentrated stress at the contact point, and complex thermal gradients, often leading to unreliable joints and loose connections.

The quality of a resistance weld is predominantly governed by the thermal cycle experienced by the material, which is controlled by process parameters such as current, time, and force. Advanced techniques like current pulsation and workpiece preheating have shown promise in managing this thermal cycle more effectively [1, 2]. The resulting thermal history directly dictates the weld nugget formation, the extent of the Heat-Affected Zone (HAZ), and the development of residual stresses, all of which are critical for the joint's final mechanical integrity [3–5].

Austenitic stainless steels, such as AISI 316L, are widely used in demanding environments due to their excellent corrosion resistance and mechanical properties. However, their performance is highly sensitive to the thermal history imposed by welding [5–7]. Exposure to specific temperature ranges can induce detrimental microstructural changes, such as sensitization (precipitation of chromium carbides at grain boundaries), which severely compromises corrosion resistance [8–10]. Additionally, the formation of brittle intermetallic phases and excessive grain growth can degrade mechanical strength and ductility [11, 12]. Therefore, achieving a controlled and optimized thermal cycle is crucial when welding AISI 316L components, especially in challenging geometries.

Pulsed current welding is an advanced strategy that offers superior control over the heat input profile [1]. By replacing a continuous current with a series of short, high-intensity pulses, this technique can localize energy deposition [13–15]. The hypothesis is that pulsation promotes a more concentrated thermal field at the challenging point-to-back interface, potentially leading to a more robust nugget, a steeper thermal gradient, and a reduced HAZ [16, 17]. Simultaneously, preheating the workpiece is a established method to mitigate issues arising from high thermal gradients [18, 19]. By raising the initial temperature of the base metal, preheating can reduce cooling rates, lower residual stresses, and decrease the risk of cracking, thereby facilitating a more uniform plastic deformation and stronger joint [20, 21].

While the individual effects of pulsed current and preheating have been explored in conventional welding, their synergistic interaction in the context of a reverse (point-to-back) resistance welding setup for fine AISI 316L wires remains largely unexplored. A systematic investigation is necessary to quantify how these parameters collectively influence critical outcomes like shear-tensile strength and HAZ characteristics in this inherently asymmetric configuration.

Therefore, this study employs an integrated experimental and numerical approach to systematically investigate the effects of two key input parameters—pulsed current frequency and preheating temperature—on the quality of reverse resistance-welded AISI 316L stainless steel wedge wires. The primary output responses critically analyzed include temperature distribution, heat-affected zone (HAZ) characteristics, and shear-tensile strength. A comprehensive Design of Experiments (DOE) is utilized to not only evaluate the individual effects of these inputs but also to uncover their synergistic interactions. The ultimate goal is to quantitatively correlate the input process parameters with the output responses to identify an optimal welding window. This optimized condition aims to overcome the persistent challenge of loose connections in point-to-back wire welding by simultaneously achieving superior joint strength and minimized microstructural degradation.

2. Methods

This study employs an integrated experimental and numerical approach to systematically investigate the effects of pulsation frequency and preheating temperature on the quality of resistance-welded AISI 316L stainless steel wires. The methodology is designed to quantitatively analyze key performance metrics, including shear-tensile strength and heat-affected zone (HAZ) characteristics, thereby establishing a correlation between process parameters and weld integrity.

2.1. Experiments

The experimental phase was conducted using AISI 316L stainless steel wedge-shaped wires, configured in a reverse welding setup as depicted in the accompanying figure. This specific workpiece geometry was selected to simulate a challenging joint configuration prevalent in practical applications, where asymmetric contact and stress distribution are critical factors. The experimental procedure encompassed shear-tensile testing to determine the mechanical strength of the welds and metallographic examination to measure the HAZ depth. For the shear-tensile tests, specimens were sectioned to isolate a single weld joint, ensuring that the measured strength accurately reflected the connection's integrity (Fig. 1). Subsequently, select samples were prepared for microscopic analysis, where the HAZ dimensions were investigated using optical microscopy to assess microstructural changes induced by the thermal cycling during welding.

Fig. 1. Wedge wires, reverse welding

The welding process was characterized by two fixed parameters: a constant electrical current of 7 kA and a welding time of 25 cycles [1, 13, 22–24]. The primary variables investigated were pulsation frequency and preheating temperature. Distinct electrical current profiles were utilized, ranging from a continuous current (0 Hz) to pulsed regimes with frequencies of 1 Hz, 5 Hz, and 10 Hz, to study the effect of energy pulsation on weld quality. Prior to welding, a controlled preheating protocol was implemented, employing a temperature-controlled hot air gun to elevate the weld zone temperature from ambient (25°C) up to 200°C. This was followed by a 3-minute heat soak period to ensure uniform thermal distribution, with verification via an infrared pyrometer, establishing a consistent and repeatable initial thermal state for all experiments.

2.2. Experimental tests

The experimental procedure was designed to quantitatively evaluate the mechanical and microstructural integrity of the AISI 316L wedge wire joints produced under varying welding conditions. To assess the weld strength, samples were carefully sectioned to isolate a single welded connection, ensuring that the measured force directly reflected the bond quality. These specimens (Fig. 2) were then subjected to shear-tensile testing to determine the maximum load-bearing capacity before failure. In parallel, selected welded samples were prepared for metallographic examination (Fig. 3). After mounting, grinding, and polishing, the cross-sections were observed using an optical microscope to measure the depth of the Heat-Affected Zone (HAZ). This two-pronged experimental approach provided critical, measurable outputs (shear-tensile strength and HAZ depth) that directly correlated the welding parameters (pulsation frequency and preheat temperature) with the final weld quality.

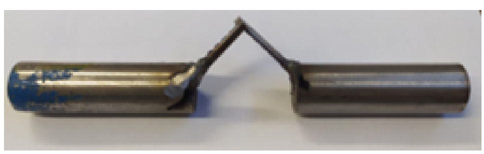

Fig. 2. The prepared shear-tensile test specimen

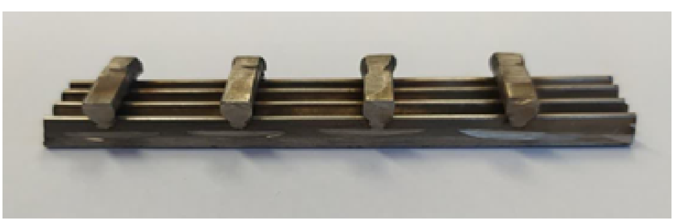

Fig. 3. The portion of the filter for metallographic purposes

2.3. Design of experiments

A structured Design of Experiments (DOE) approach was employed to systematically investigate the individual and combined effects of the two key process parameters: preheating temperature and pulsation frequency. The experimental design was formulated as a full factorial design, considering all possible combinations of the selected factor levels. This approach allows for a comprehensive analysis of the main effects of each parameter as well as any potential interaction effects between them.

The factors and their respective levels were chosen as follows:

- **Preheating Temperature (°C):** Four levels were selected: 50°C, 100°C, 150°C, and 200°C. This range was chosen to evaluate the impact of initial thermal energy on the welding process, from a moderate preheat to a significantly elevated temperature.
- **Pulsation Frequency (Hz):** Four levels were selected: 0 Hz (representing continuous current), 1 Hz, 5 Hz, and 10 Hz. This range was chosen to study the transition from conventional welding to a pulsed regime with varying degrees of energy interruption.

The combination of these four levels for each factor resulted in a total of 16 unique experimental runs, as systematically presented in Table 1. For each of these 16 runs, the corresponding outcomes (namely, the shear-tensile strength (from both FEA and experimental data) and the maximum HAZ depth (also from both FEA and experimental data)) were measured and recorded. This structured design enables a robust statistical analysis to identify optimal process conditions and understand the relationship between the input parameters and the output responses.

2.4. Finite element analysis

To complement the experimental findings and gain deeper insight into the thermomechanical phenomena during welding, a Finite Element Analysis (FEA) model was developed. The numerical simulation replicated the entire process sequence: the application of a pulsed current and preheating during the welding phase, a subsequent short cooling period, and finally, a simulated tensile test on the welded assembly (Fig. 4). The model calculated key outputs such as temperature distribution, residual stress development, and the stress state during mechanical loading. The primary goal of this numerical study was to validate the experimental trends by comparing simulated results (e.g., shear-tensile strength and HAZ depth) with measured data. Furthermore, the FEA provided detailed visualizations, such as contour plots of stress offering a fundamental understanding of how pulsed current concentrates heat and how preheating homogenizes the thermal field, which directly influences joint strength and microstructural damage.

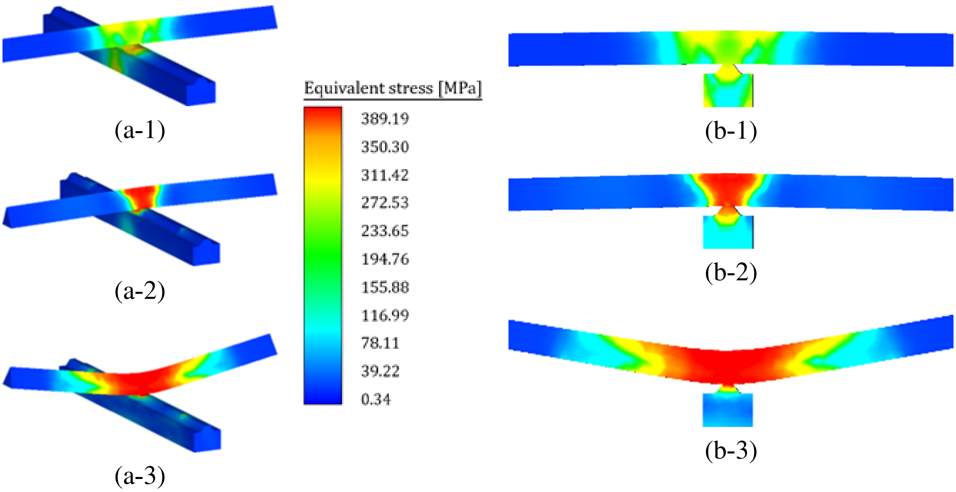

Fig. 4. Analytical shear-tensile test configuration: (a) 3D view; (b) cross-section; (1) at the end of the welding; (2) before tensile test (maximum residual stress) (3) at the end of the tensile test

3. Results and discussion

The comprehensive results obtained from the 16-run DOE, as systematically presented in Table 1, provide a clear and quantitative overview of how the two key process parameters (preheating temperature and pulsation frequency) influence the

Table 1. The factors and levels in DOE together with the obtained results

Run No.	Preheating temperature (°C)	Freq. (Hz)	Shear-tensile strength (MPa)		Max. HAZ depth (mm)	
			FEA	Exp.	FEA	Exp.
0	50	0	389.19	377.52	2.22	2.24
1	50	1	389.79	397.59	2.06	2.12
2	50	5	391.04	383.22	2.00	1.96
3	50	10	392.20	388.28	1.97	1.99
4	100	0	407.87	399.71	2.16	2.20
5	100	1	408.47	404.38	2.00	2.06
6	100	5	409.72	422.01	1.95	1.93
7	100	10	410.87	402.66	1.92	1.82
8	150	0	418.55	410.17	2.14	2.12
9	150	1	419.15	419.15	1.98	2.04
10	150	5	420.40	416.19	1.93	1.83
11	150	10	421.55	429.98	1.90	1.99
12	200	0	428.52	445.66	2.13	2.08
13	200	1	429.12	411.96	1.97	2.03
14	200	5	430.37	417.46	1.91	1.91
15	200	10	431.53	427.21	1.88	1.83

primary outcomes of the resistance welding process: shear-tensile strength and Heat-Affected Zone (HAZ) depth.

The data in Table 1 allow for a direct comparison between the numerical predictions from the Finite Element Analysis (FEA) and the experimental measurements. This side-by-side presentation is crucial for validating the computational model. A general observation from the table is the strong correlation between the FEA and experimental results for both output responses. The values for shear-tensile strength and maximum HAZ depth from the simulations consistently align closely with the empirical data across most of the 16 conditions. This close agreement confirms the accuracy and reliability of the FEA model in capturing the essential physics of the welding process, thereby establishing it as a valuable tool for predicting weld performance.

Furthermore, the structured design of the table immediately reveals overarching trends. For instance, it is readily apparent that increases in preheating temperature (moving down the table within a frequency group) generally correspond to higher values in the shear-tensile strength columns. Similarly, increases in pulsation frequency (moving right across the table within a temperature group) are generally associated with a decrease in the maximum HAZ depth values. These initial observations confirm the individual and combined roles of preheating and pulsation in simultaneously enhancing mechanical strength and controlling microstructural damage. The following sections will provide a detailed analysis and discussion of these trends and their underlying mechanisms.

3.1. Shear-tensile strength

As illustrated in Fig. 5, the numerical results of the shear-tensile test demonstrate a clear trend of increasing maximum shear-tensile strength with rising pulsation frequency. The strength is measured at a critical moment just before separation occurs, ensuring consistent and comparable deformation across all samples. At this point, the weld joint tolerates the highest applied stress without failing. The increase in strength with frequency is directly correlated with the stress distribution observed in the contours; higher frequencies lead to a more concentrated and intense stress region at the weld interface, indicating that the alloy undergoes less widespread plastic deformation and bears higher stress more efficiently. This localized stress concentration, resulting from the pulsed current's ability to concentrate thermal energy and refine the weld nugget, effectively enhances the joint's load-bearing capacity, thereby increasing the maximum shear-tensile strength.

As demonstrated in Fig. 6, the numerical results reveal a positive correlation between the preheat temperature and the maximum shear-tensile strength of the weld joint. The contour plots show that with an increase in preheat temperature from 25°C to 200°C, the stress distribution becomes more favorable. Specifically, a higher preheat temperature reduces the severity of stress concentration at the weld interface and promotes a more uniform distribution of stress. This allows the joint

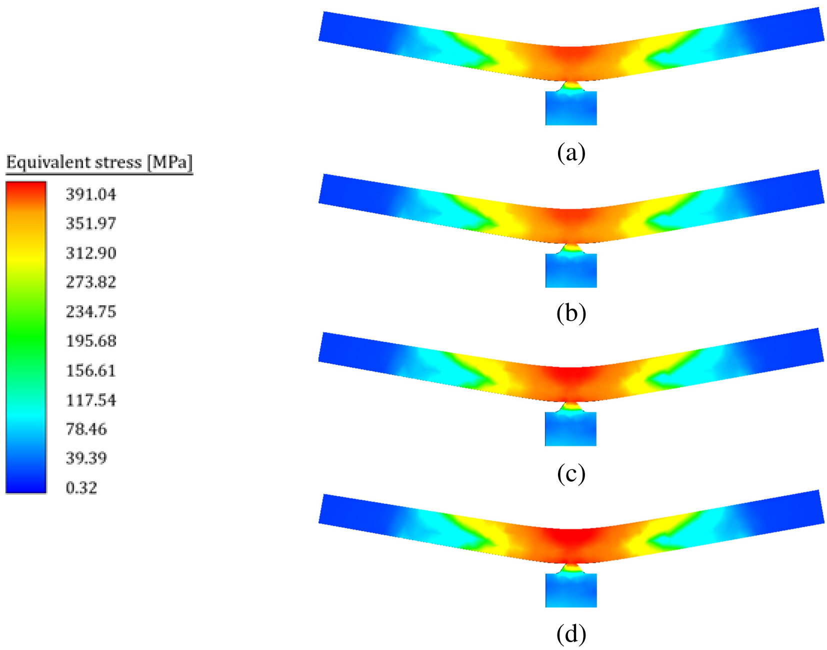

Fig. 5. Numerical results of maximum shear-tensile strength vs. frequency: (a) $f = 0$; (b) $f = 1$ Hz; (c) $f = 5$ Hz; (d) $f = 10$ Hz

to tolerate a higher applied load before failure. The underlying mechanism is that preheating lowers the thermal gradient during welding, reducing residual stresses and minimizing the risk of brittle microstructural formations. Consequently, the alloy exhibits enhanced ductility and strength, bearing more stress with less localized deformation, which is quantified as an increase in the maximum shear-tensile strength.

Fig. 7 and Fig. 8 quantitatively illustrate the individual and significant effects of pulsation frequency and preheat temperature on the shear-tensile strength. Figure 6 demonstrates that at a constant preheat temperature of 25°C, increasing the pulsation frequency leads to a consistent and notable rise in the shear-tensile strength. This improvement is directly attributed to the fundamental mechanism of pulsed current welding: the short, high-energy pulses confine heat generation to the weld interface, creating a steeper thermal gradient. This concentration of energy promotes the formation of a more robust and finer-grained nugget while simultaneously minimizing the extent of the HAZ. The resultant weld is thus stronger and more resistant to shear forces. Conversely, Fig. 7 shows that even with a continuous current ($f = 0$ Hz), elevating the preheat temperature from 25°C to 200°C significantly enhances the joint strength. The underlying reason for this enhancement is that preheating raises the initial energy state of the material, reducing the severe temperature difference between the weld zone and the base metal during the

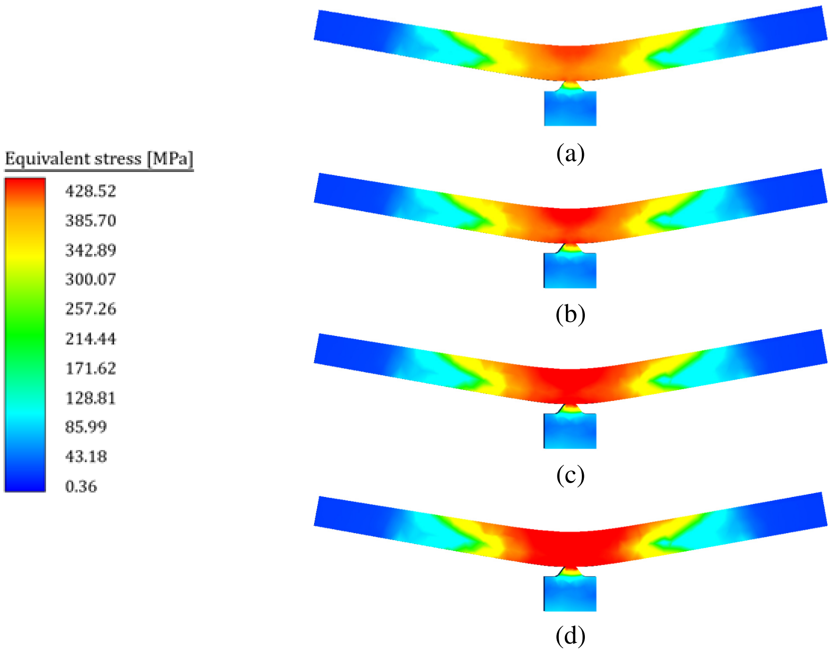

Fig. 6. Numerical results of maximum shear-tensile strength vs preheat temperature: (a) $T_P = 25^{\circ}$C; (b) $T_P = 100^{\circ}$C; (c) $T_P = 150^{\circ}$C; (d) $T_P = 200^{\circ}$C

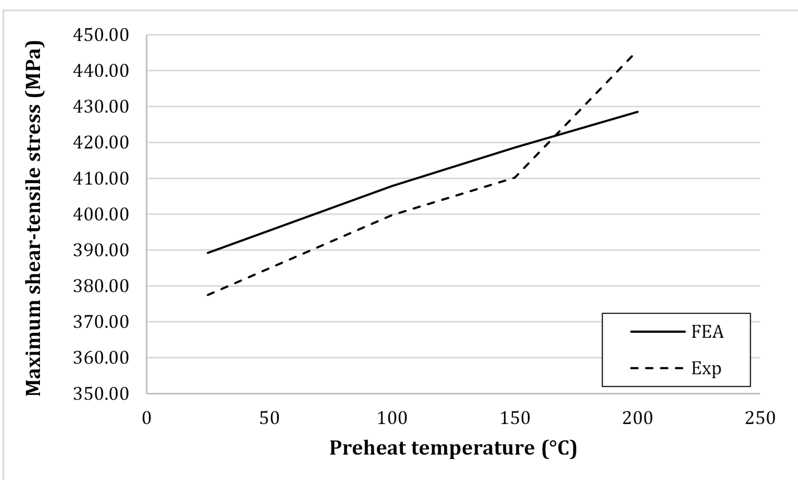

Fig. 7. Shear-tensile strength vs. frequency ($T_P = 25^{\circ}$C)

welding process. This mitigation of the thermal gradient leads to slower cooling rates and a reduction in residual stresses, thereby minimizing the risk of cracking and allowing the material to deform more plastically, ultimately resulting in higher load-bearing capacity before failure. Together, these figures confirm that while both higher pulsation frequency and increased preheat temperature are effective, independent strategies for improving strength, they achieve this through distinct thermal management mechanisms—frequency by localizing energy and preheating by homogenizing the thermal field.

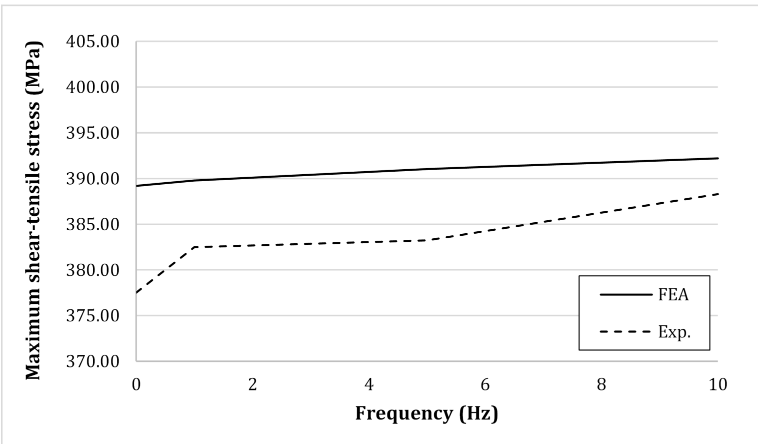

Fig. 8. Shear-tensile strength vs. pre-heat temperature ($f = 0$)

3.2. Heat-affected zone

Fig. 9 illustrates the relationship between pulsation frequency and the maximum depth of the Heat-Affected Zone (HAZ) at a constant preheat temperature of 25°C. A clear decreasing trend is observed; as the pulsation frequency increases from 0 Hz (continuous current) to 10 Hz, the maximum HAZ depth consistently reduces. This reduction is attributed to the localized energy deposition characteristic of pulsed current welding. The short, high-intensity pulses confine heat generation primarily to the weld interface, creating steeper thermal gradients and limiting the lateral and axial conduction of heat into the base metal. Consequently, the volume of material exposed to temperatures sufficient to cause microstructural alterations is minimized, resulting in a narrower HAZ.

Fig. 10 demonstrates the effect of preheat temperature on the maximum HAZ depth when using a continuous current (0 Hz). Contrary to the effect of pulsation, increasing the preheat temperature from 25°C to 200°C leads to a slight increase in the measured HAZ depth. This occurs because preheating raises the initial thermal energy of the entire workpiece. During welding, this elevated baseline temperature reduces the thermal gradient between the weld zone and the surrounding material,

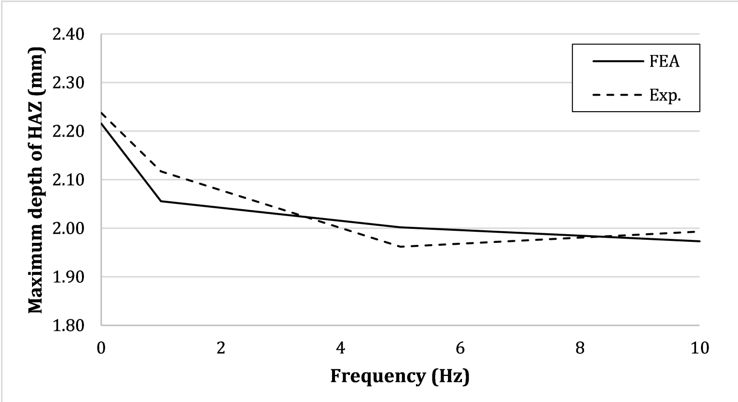

Fig. 9. Maximum HAZ depth vs. pulse frequency ($T_P = 25°C$)

allowing heat to diffuse more readily and over a broader area. While beneficial for reducing residual stresses and cracking risk, this more uniform thermal field can extend the region experiencing microstructural changes, thus widening the HAZ when pulsation is not employed to counterbalance the effect.

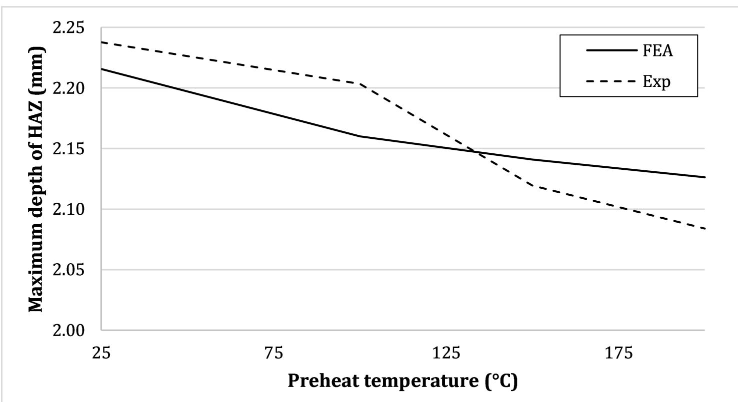

Fig. 10. Maximum HAZ depth vs. pre-heat temperature ($f = 0$)

Fig. 11 provides a direct visual correlation between the simulated thermal fields and the experimentally observed HAZ. The cross-sectional temperature contours from the Finite Element Analysis (FEA) clearly show how the isotherms contract with increasing pulsation frequency (sub-figures a-1 to a-4), confirming the mechanism of energy concentration and the consequent reduction in the thermal spread. The superimposed micrographs in Fig. 11 demarcate the actual HAZ boundaries, which align closely with the lower-temperature isotherms (near the sensitization range for AISI 316L) predicted by the FEA model. This synergy between numerical simulation and experimental measurement validates that the HAZ extent is primarily governed by the spatial distribution and duration of critical temperatures, which are effectively controlled by the combined parameters of pulsation frequency and preheat temperature.

3.3. Temperature

3.3.1. Distribution

The transient thermal fields presented in Fig. 11 quantitatively demonstrate the significant impact of pulsation frequency and preheating on the welding process. The sequence from Fig. 11(a-1) to (a-4) reveals that transitioning from a continuous current (0 Hz) to a pulsed regime at 3 Hz results in a more concentrated and intense thermal gradient. This is evidenced by a noticeable contraction of the lower-temperature isotherms, corresponding to a reduced HAZ. The concentration

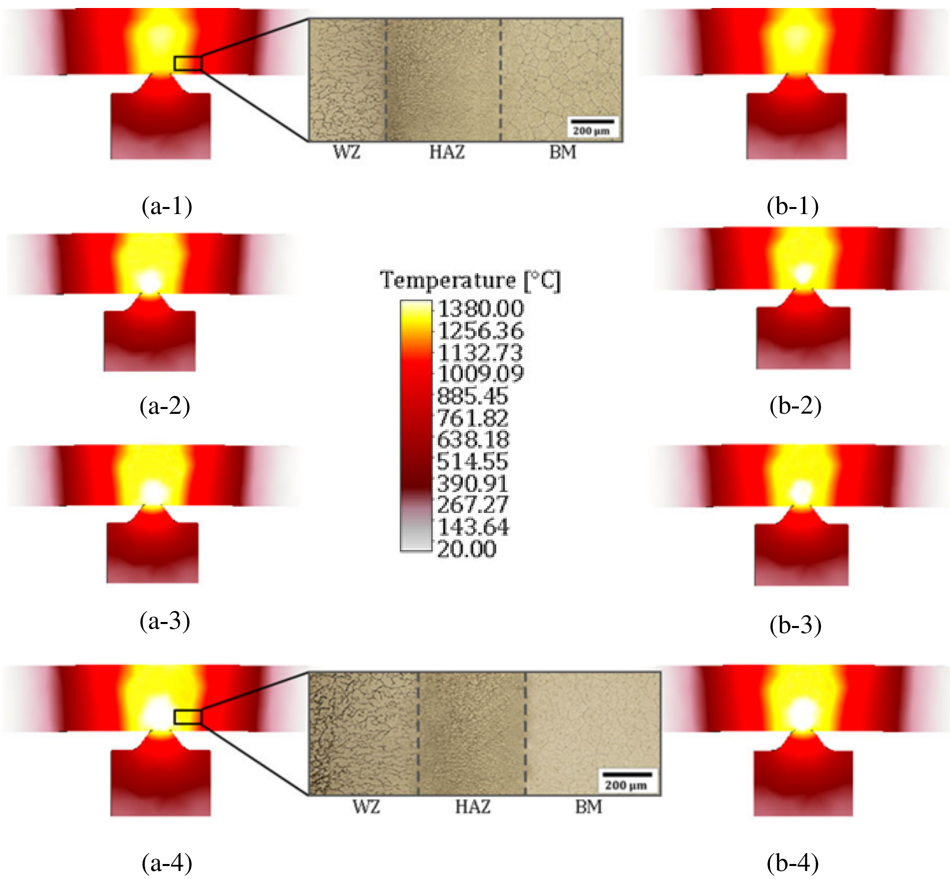

Fig. 11. Thermal Field Evolution under Pulsed Welding Parameters. Cross-sectional views of temperature distribution, showing the influence of pulsation frequency and preheating temperature, together with micrographs indicating the spread of HAZ: (a-1) $f = 0$; (a-2) $f = 2$ Hz; (a-3) $f = 5$ Hz; (a-4) $f = 10$ Hz; (b-1) $T_P = 25^{\circ}$C; (b-2) $T_P = 100^{\circ}$C; (b-3) $T_P = 150^{\circ}$C; (b-4) $T_P = 200^{\circ}$C (WZ: Weld zone, BM: Base metal)

of energy during each pulse elevates the peak temperature at the weld centerline while simultaneously reducing the duration of exposure for the surrounding material to critical intermediate temperatures (550–850°C for AISI 316 steel), thereby mitigating microstructural damage such as sensitization. Concurrently, the progression in Fig. 11(b-1) to to (b-4) indicates that an elevated preheating temperature raises the overall baseline thermal energy of the workpiece. This broader initial heat distribution facilitates a more uniform thermal diffusion during welding, which can help reduce residual stresses and the risk of cracking, albeit potentially widening the HAZ if not carefully balanced with the pulsation parameters. Collectively, these results underscore that a synergistic combination of optimized pulse frequency and controlled preheating provides a powerful method for tailoring the thermal cycle to achieve a desirable weld profile with minimized microstructural degradation.

When comparing pulsed and continuous welding currents under conditions of identical total weld cycle time and constant current amplitude during active phases, the pulsed current method demonstrably yields a smaller Heat-Affected Zone (HAZ) and can achieve a higher peak interfacial temperature. This phenomenon is primarily governed by two synergistic mechanisms: thermal energy localization and the inter-pulse residual heat effect.

Firstly, the pulsed current strategy capitalizes on thermal energy localization. In the continuous current mode, energy is input steadily, allowing heat sufficient time to diffuse radially and axially into the base metal, thereby creating an extensive HAZ. In contrast, the pulsed mode distributes the same total "on-time" into short, high-intensity bursts separated by off-time periods. During each off-time interval, heat generated at the interface does not have sufficient time to penetrate deeply into the base metal. Instead, it is efficiently conducted towards the water-cooled electrodes, effectively "trapping" the thermal energy within a more confined volume around the weld interface for the subsequent pulse. This cyclic process creates a steeper thermal gradient, concentrating the thermal energy and leading to a higher peak temperature at the weld center while restricting the lateral spread of heat, thereby minimizing the HAZ.

Secondly, the process benefits from an intrinsic inter-pulse annealing or preheating effect. Each current pulse elevates the temperature of a localized volume. This temperature increase raises the local electrical resistivity of the material. Since Joule heating is proportional to the square of the current and the resistivity (I^2R), the subsequent pulse encounters a region of higher resistance, resulting in more efficient heat generation within the intended weld zone itself. This cyclic build-up of residual heat ensures that a larger fraction of the input energy is utilized for nugget formation rather than heating the surrounding base metal. Consequently, for an equivalent total cycle time and current amplitude, the pulsed schedule achieves deeper penetration and a more robust nugget with less overall thermal input to the workpiece, leading to a superior combination of joint strength and a minimized, less microstructurally degraded HAZ.

For AISI 316 stainless steel, the Heat-Affected Zone (HAZ) is vulnerable to significant microstructural degradation across specific temperature ranges. Exposure to the sensitization range of 425–850°C promotes the precipitation of chromium carbides at grain boundaries, severely impairing corrosion resistance, with the most critical effects occurring between 600–800°C. Furthermore, sustained temperatures within the 600–900°C window can facilitate the formation of a brittle sigma phase, which drastically reduces material toughness. At even higher temperatures, typically above 900°C, recrystallization and excessive grain growth take place, leading to a deterioration of mechanical strength. Therefore, controlling the thermal cycle to minimize the HAZ's time in these critical ranges is paramount for preserving the material's intrinsic corrosion resistance and mechanical integrity.

3.3.2. Maximum temperature

Fig. 12 illustrates the relationship between pulsation frequency and the maximum temperature achieved at the weld interface, parameterized by preheat temperature. A consistent, non-linear increasing trend is observed across all preheat levels. At lower preheat temperatures (25°C and 100°C), the maximum temperature shows a strong sensitivity to frequency, rising sharply as frequency increases from 0 Hz to 5 Hz. This is a direct result of the energy concentration effect inherent to pulsed current welding; shorter, more frequent bursts of energy reduce heat dissipation to the surrounding base metal, leading to more efficient and localized heating. However, the rate of temperature increase diminishes significantly between 5 Hz and 10 Hz, indicating a trend towards thermal saturation. For higher preheat temperatures (150°C and 200°C), the system reaches its apparent peak temperature of 1380°C at a lower frequency (5 Hz). This occurs because the combination of high initial thermal energy and pulsed energy input quickly drives the system to its maximum thermal capacity, beyond which additional pulsing cannot raise the

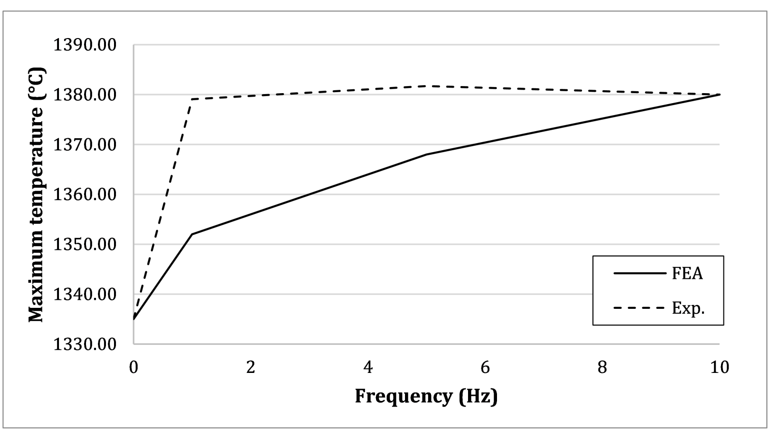

Fig. 12. Maximum temperature vs. frequency

temperature further. This saturation phenomenon underscores the existence of a practical upper limit for heat input in this process.

Fig. 13 demonstrates the influence of preheat temperature on the maximum weld temperature, with frequency as a parameter. A positive correlation is evident for all frequency settings, confirming that a higher initial thermal state consistently results in a higher peak temperature. The sensitivity to preheat is most pronounced at lower frequencies (0 Hz and 1 Hz), where the thermal curve is steepest. In these regimes, the energy input from welding alone is less concentrated, making the system more reliant on the initial energy provided by preheating to achieve higher peak temperatures. Conversely, at high frequencies (5 Hz and 10 Hz), the curves flatten rapidly as the preheat temperature increases. The highly concentrated energy from pulsing becomes the dominant factor, quickly driving the temperature to the 1380°C ceiling. For instance, at 10 Hz, even a moderate preheat of 100°C is sufficient to reach the maximum temperature, and further preheating provides no additional benefit. This illustrates that preheating and pulsation frequency are synergistic parameters; preheating is most impactful when the welding process itself is less efficient (low frequency), while its utility diminishes when using highly efficient, high-frequency pulsation.

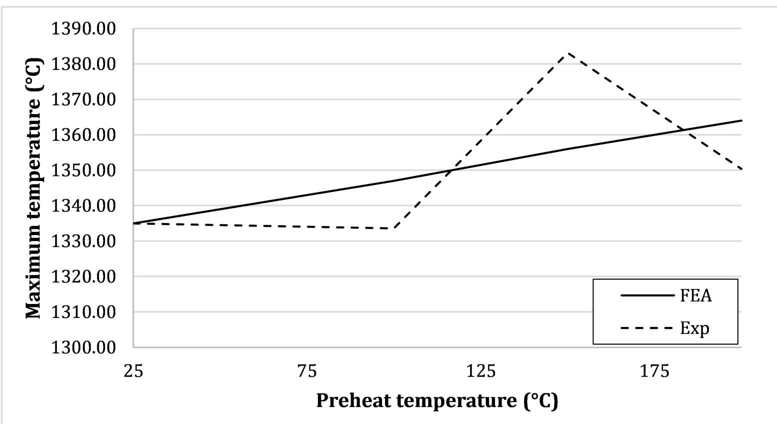

Fig. 13. Maximum temperature vs. pre-heat temperature

4. Conclusions

This study systematically investigated the synergistic effects of pulsed current frequency and preheat temperature on the weld strength and microstructural integrity of AISI 316L stainless steel wedge wires in a reverse (point-to-back) resistance welding setup. Based on the integrated experimental and numerical analysis, the following conclusions can be drawn:

- Pulsed current frequency significantly enhances joint strength and refines the weld zone. Increasing the pulsation frequency (0–10 Hz) leads to a more concentrated thermal energy deposition at the weld interface, resulting in a finer-grained weld nugget and reduced Heat-Affected Zone (HAZ) depth. This localized energy input improves shear-tensile strength by promoting a more robust joint with minimal microstructural degradation.

- Preheating temperature improves weld integrity by mitigating thermal gradients. Elevated preheat temperatures (50–200°C) reduce cooling rates, lower residual stresses, and minimize the risk of cracking. This leads to more uniform plastic deformation and higher load-bearing capacity, as evidenced by increased shear-tensile strength values across all tested conditions.
- Synergistic interaction between pulsation and preheating optimizes weld quality. The combined application of optimized pulsed current (e.g., 10 Hz) and moderate preheating (150–200°C) yields the best balance between mechanical performance and microstructural preservation. This synergy effectively addresses the challenges of asymmetric heat distribution and loose connections inherent to point-to-back welding configurations.
- Numerical modeling validates experimental trends with high accuracy. Finite Element Analysis (FEA) predictions for shear-tensile strength and HAZ depth closely match experimental measurements, confirming the reliability of the model for process optimization and parameter selection in similar welding applications.
- Controlled thermal management is critical for AISI 316L welding. Minimizing exposure to critical temperature ranges (425–850°C) through pulsed current and preheating strategies effectively prevents sensitization, sigma phase formation, and excessive grain growth, thereby preserving the corrosion resistance and mechanical properties of the stainless steel.

AI Assistance Disclosure

During the preparation of this work, the author(s) used DeepSeek AI to improve readability, language clarity, and grammatical accuracy. After using this tool/service, the author(s) reviewed and edited the content as needed and take(s) full responsibility for the content of the publication.

Conflict of Interest

The authors declare that they have no conflict of interest.

Data Availability statement

The raw simulation data (including finite element model files, input parameters, and detailed output results) that support the findings of this study are available from the corresponding author upon a reasonable request.

References

[1] M. Jafari Vardanjani, and J. Senkara. Effect of Multi-Pulsed Current Mechanism on Shunting Current in Resistance Spot Welding (RSW) of AA-2219 Sheets. *Experimental Techniques*, 1–15, 2021, doi: 10.1007/s40799-021-00504-x.

[2] M. Jafari Vardanjani, A. Araee, J. Senkara, J. Jakubowski, and J. Godek. Experimental and numerical analysis of shunting effect in resistance spot welding of Al2219 sheets. *Bulletin of the Polish Academy of Sciences, Technical Sciences*, 64(2), 2016, doi: 10.1515/bpasts-2016-0048.

[3] J. Gould. An examination of nugget development during spot welding, using both experimental and analytical techniques. *Welding Journal*, 66(1): 1-s-10-s, 1987, doi: 10.22059/j-camech.2015.53389.

[4] M. Jafari Vardanjani, A. Araee, J. Senkara, J. Jakubowski, and J. Godek. Metallurgical Effects of Shunting Current on Resistance Spot-Welded Joints of AA2219 Sheets. *Journal of Materials Engineering and Performance*, 25(8):3506–3517, 2016. doi: 10.1007/s11665-016-2168-3.

[5] T.-L. Lv, Y.-Z. Rao, Q.-X. Zhang, Y.-J. Xia, Y. Lin, F. Wu, Y.-B. Li, and D.-J. Yan. Effect of storage time on the surface status and resistance spot weldability of TiZr pretreated 5182 aluminum alloy. *Journal of Manufacturing Processes*, 81:166–176, 2022. doi: 10.1016/j.jmapro.2022.06.058.

[6] P. Podržaj and S. Simončič. Temperature measurement during resistance spot welding using a digital camera. In: *2013 IEEE International Conference on Mechatronics and Automation*, pages 1305–1310, 4-7 Aug. 2013. doi: 10.1109/ICMA.2013.6618102.

[7] R.N. Raoelison, A. Fuentes, C. Pouvreau, Ph. Rogeon, P. Carré, and F. Dechalotte. Modeling and numerical simulation of the resistance spot welding of zinc coated steel sheets using rounded tip electrode: Analysis of required conditions. *Applied Mathematical Modelling*, 38(9):2505–2521, 2014. doi: 10.1016/j.apm.2013.10.060.

[8] M. Jafari Vardanjani, A. Araee, J. Senkara, M. Sohrabian, and R. Zarandooz. Influence of Shunting Current on the Metallurgical and Mechanical Behaviour of Resistance Spot-welded Joints in AA2219 Joints. *Strojniski Vestnik – Journal of Mechanical Engineering*, 62(11):11, 2016. doi: 10.5545/sv-jme.2016.3682.

[9] Y. Yang, Y. Li, J. Bi, H. Liu, S. Ao, and Z. Luo. Microstructure and mechanical properties of 2195/5A06 dissimilar joints made by resistance spot welding. *Materials Characterization*, 191:112147, 2022. doi: 10.1016/j.matchar.2022.112147.

[10] H. Zhang, J. Senkara, and X. Wu. Suppressing cracking in resistance welding AA5754 by mechanical means. *J. Manuf. Sci. Eng.*, 124(1):79–85, 2002. doi: 10.1115/1.1418693.

[11] H. Zhang and J. Senkara. *Resistance Welding: Fundamentals and Applications*. Second Edition, CRC Press, Place, 2011.

[12] Q. Zhao, H. Wu, X. Chen, Y. Ni, X. An, W. Wu, and T. Zhao. Insights into the structural design strategies of multi-spot ultrasonic welded joints in thermoplastic composites: A finite element analysis. *Composite Structures*, 299:115996, 2022. doi: 10.1016/j.compstruct.2022.115996.

[13] S. Amini and M. Jafari Vardanjani. Effect of the time intervals on the mechanical and metallurgical quality of AA-2219 resistance spot weld joints. *Proceedings of the Institution of Mechanical Engineers, Part E: Journal of Process Mechanical Engineering*, 2025. doi: 10.1177/09544089251321594.

[14] M. Jafari Vardanjani, A. Araee, J. Senkara, J. Jakubowski, and J. Godek. Theoretical analysis of shunting effect in resistance spot welding (RSW) of AA2219. *Journal of the Chinese Institute of Engineers*, 39(8):907–918, 2016. doi: 10.1080/02533839.2016.1215940.

[15] R. Moharrami and B. Hemmati. Numerical stress analysis in resistance spot-welded nugget due to post-weld shear loading. *Journal of Manufacturing Processes*, 27:284–290, 2017. doi: 10.1016/j.jmapro.2017.05.007.

[16] T. Loulou, P.L. Masson, and P. Rogeon. Thermal characterization of resistance spot welding. *Numerical Heat Transfer, Part B: Fundamentals*, 49(6):559–584, 2006. doi: 10.1080/10407790500433986.

[17] S. Raj and P. Biswas. Effect of induction preheating on microstructure and mechanical properties of friction stir welded dissimilar material joints of Inconel 718 and SS316L. *CIRP Journal of Manufacturing Science and Technology*, 41:160–179, 2023. doi: 10.1016/j.cirpj.2022.12.014.

[18] R.M. Choudhari, A.M. Adhaye, M.M. Patil, and V.N. Sulakhe. Resistance Spot Welding Process Mechanisms and Influencing Parameters: Literature Review. In: *Advances in Materials and Manufacturing*, pages 335–346, Singapore, 2025. doi: 10.1007/978-981-96-7659-0.

[19] V. Feizollahi, A. Bahmani, N. Nadimi, M. Reza Salmani, M. Pouranvari, Y.-D. Park, and R. Ashiri. Factors affecting weld quality in resistance spot welding of advanced high strength steels. *Scientific Reports*, 15(1):30012, 2025. doi: 10.1038/s41598-025-14174-x.

[20] S. Durnagöz, M. Mayer, and M.F. Huber. An Approach for Expulsion Predicting in Resistance Spot Welding. Procedia CIRP, 130:1732–1738, 2024. doi: 10.1016/j.procir.2024.10.308.

[21] D. Zhao, N. Vdonin, L. Radionova, L. Glebov, and V. Ivanov. Optimisation of welding parameters for ultrasonically assisted resistance spot welding of pure titanium Grade 2 and aluminium alloy 5754. *International Journal of Lightweight Materials and Manufacture*, 2025. doi: 10.1016/j.ijlmm.2025.09.005.

[22] J. Shen, Y. Zhang, X. Lai, and P.C. Wang. Modeling of resistance spot welding of multiple stacks of steel sheets. *Materials & Design*, 32(2):550–560, 2011. doi: 10.1016/j.matdes.2010.08.023.

[23] A. Singh Bharaj, A. Kewati, S. Shukla, S. Gedam, R. Kukde, and S. Verulkar. Study of resistant spot welding and its effect on the metallurgical and mechanical properties – a review. *Materials Today: Proceedings*, 2023. doi: 10.1016/j.matpr.2023.04.650.

[24] B. Wang, L. Hua, X. Wang, and J. Li. Effects of multi-pulse tempering on resistance spot welding of DP590 steel. *The International Journal of Advanced Manufacturing Technology*, 86(9):2927–2935, 2016. doi: 10.1007/s00170-016-8361-6.